STATIC AND DYNAMIC MEASUREMENTS OF RESERVOIR HETEROGENEITIES IN CARBONATE RESERVOIRS

Shameem Siddiqui, James Funk, and Aon Khamees
Saudi Aramco Lab R&D Center, Dhahran, Saudi Arabia

Abstract

Heterogeneity plays a critical role in determining the recovery from petroleum reservoirs. The determination of heterogeneities can be classified into static and dynamic techniques. CT and NMR techniques provide excellent means to determine the mobile fluid behavior and the interactions of these mobile fluids with the confining surfaces of the pores. However, few studies have focused on the use of the interrelations of slice distributions determined from these techniques.

In the present work, static heterogeneities were determined from distributional measurements of core petrophysical properties including conventional whole core and plug data, profile permeametry measurements, CT number distributions and NMR T_2 distributions. CT monitoring of displacement fronts during various stages of multi-phase coreflood tests provided the dynamic measurements. Ambient condition coreflooding studies on a three-plug composite core were conducted to show the dependence of fluid displacements on the microscopic heterogeneities existing in the core. The slice-by-slice distributional data (porosity, permeability and saturation) in the horizontal direction were used to visualize the position dependent variations. These were then compared with standard heterogeneity parameters (Lorenz and Dykstra-Parsons) for both the discrete samples and the reservoir interval. Results showed that simple porosity-mapped heterogeneity indicators are unable to capture the variability in saturation distributions for typical carbonate samples. However, even at the plug scale, expected deviations about a mean value can be established based on the relative position of heterogeneities and standard heterogeneity coefficients for the reservoir interval.

Introduction

Computerized Tomography (CT) is a non-destructive imaging technique that utilizes X-ray technology and mathematical reconstruction algorithms to view a cross-sectional slice of an object. Since the early 80's, the petroleum industry has been using CT-scanners as an effective tool for analyzing the reservoir cores. CT provides a non-destructive, non-invasive way of looking at cores and helps identify lithology, measure porosity and determine heterogeneity in three dimensions. The particular applications of CT as a rock description and core analysis tool include determination of fractures and heterogeneities, measurement of bulk density and porosity, visualization of mud invasion, characterization of lithology, evaluation of damage in unconsolidated cores and sectional analysis of cores. Apart from core characterization, CT used to visualize and quantify fluid displacement in cores (both miscible and immiscible), to determine bulk density, to determine residual oil saturation and trapped porosities, to visualize and quantify gravity

and viscous effects, etc. CT is mostly used for the determination of phase saturations in the porous media. Detailed reviews of the application of CT in various coreflood experiments can be found in the literature (Kantzas, 1990; Siddiqui, 1994).

Nuclear Magnetic Resonance (NMR) technology has been in use in the medical industry for almost twenty years and like the CT it has been picked up by the oil industry to look inside the fluid-filled cores. For NMR measurements, the fluid-filled core is placed inside a sample chamber in a homogeneous magnetic field. With the application of two-dimensional magnetic field gradients, the longitudinal and transverse relaxation time curves (T_1 and T_2) are measured as a function of position. NMR measurements provide a view of the pore system based primarily on the relaxation of nuclear spins at the pore surface. This mechanism provides data that can be used to correlate with permeability. Current models for the relaxation process and the corresponding permeability transform are based on the equations first proposed by Bloembergen et al. (1948).

$$\frac{1}{T_2} = \left[\frac{1}{T_{2,Bulk}} + \frac{1}{T_{2,Diffusion}} + \frac{1}{T_{2,Surface}} \right] \quad \text{..... 1}$$

and

$$\frac{1}{T_2} = SR \times S/V \quad \text{..... 2}$$

where,

T_2 = Transverse Relaxation Time
SR = Surface Relaxivity
S/V = Surface to Volume Ratio

The S/V ratio is used as the physical basis for the permeability transform. In even the most general case, the permeability is assumed to increase as the S/V decreases. Physically, NMR measurements are exponentially decreasing alternating currents. In standard petrophysical NMR equipment these currents are in the 2-MHz frequency range. To characterize the pore system in a reservoir rock, the exponentially decreasing signal is inverted into a distribution of exponentials (T_2 times) that are considered to correspond to specific surface to volume ratio pores. In this study, the T_2 distributions are combined with CT-derived porosity distributions to characterize the heterogeneity of specific plug samples.

In reservoir characterization heterogeneity specifically applies to the variability that affects flow. Jensen et al. (1997) classified heterogeneity into two groups, static and dynamic. Static measures are based on measured samples from the formation and require some flow model to be used to interpret the effect of variability on flow. Dynamic measures use a flow experiment and are, therefore, a direct measure of how the

heterogeneity affects the flow. One of the commonly-used techniques for measuring the static heterogeneities is the Stile's Plot, which gives the Lorenz Coefficient, L_c. The technique involves ordering the product of permeability and the representative thickness (kh) in the descending order along with the corresponding porosity-representative thickness product (ϕh) for a well (or wells). The normalized cumulative values of kh, which also known as the fraction of total flow capacity (between 0 and 1) are then plotted against the normalized cumulative values of ϕh, which is also known as the fraction of the total volume (between 0 and 1). This plot is the so-called the Stile's plot. The L_c is calculated by comparing the area under the curve above a 45° line between (0,0 and 1,1) and 0.5. L_c can theoretically vary between 0 and 1, with 1 representing the highest degree of heterogeneity. According to Jensen et al. (1997), L_c offers several advantages over the other more commonly-used heterogeneity indicator, the Dykstra-Parson's coefficient. They include the fact that L_c can be calculated for any distribution (does not have to be a normal distribution), that L_c values do not depend on the best-fit procedures used and that its evaluation includes porosity heterogeneity and variable thickness layers. Details of the procedures for calculating L_c and V_{DP} can be found in the literature (Craig, 1971, Jensen et al., 1997).

The coefficient of variation, C_v is another lesser-known measure of heterogeneity. It is a dimensionless measure of sample variability or dispersion and is given by,

$$C_v = \frac{\sqrt{Var(x)}}{E(x)} \quad \text{.....3}$$

where, the numerator is the sample standard deviation and the denominator is the sample mean. C_v is being increasingly applied in geological and engineering studies as an assessment of permeability heterogeneity. For data from different populations, the mean and standard deviation often tend to change together such that C_v stays relatively constant. Any large changes in C_v between two samples indicate a dramatic difference in the populations associated with those samples (Jensen et al., 1997).

Experimental

The cores used for this paper were selected from two vertical wells (designated as Well A and Well B) from a Jurassic carbonate reservoir. Conventional core analysis work was performed on cores collected from the entire reservoir section using both 4" vertical whole core samples and 1-1/2" horizontal plugs. For the whole cores, three different air permeability measurements were made: one in the vertical direction (k_{vert}), and two others in the horizontal direction at 90 degrees to each other. The two horizontal permeability measurements are called k_{HMax} and k_{H90}, respectively in the paper, with the former being the maximum of the two permeability readings taken in any arbitrary direction.

A total of five 1-1/2" diameter carbonate plug samples from the two wells were selected for using in CT, NMR, Profile Permeametry and coreflooding studies. These are, plug

nos. 248 and 246, from Well A, and plug nos. 26, 157 and 100, from Well B. The capillary contact between two adjacent plugs was maintained by using circular filter papers. All CT-scanning work was done using a Deltascan-100 scanner (120 KHz, 25 mA, translate-rotate system). Coreflooding was conducted at room temperature and at 2500-psi overburden pressure using a special coreflooding system consisting of Quizix pumps, a Temco FCH series coreholder and a Compumotor/AcuTrac table positioning system. Figure 1 shows a simplified schematic of the coreflooding system used.

The coreflooding test sequence for the composite plug from Well B included vacuum-saturation with brine, an oilflood (stopping for scanning after 0.2-*PV*, 10-*PV* and 20-*PV* of oil injected) and a waterflood (stopping for scanning after 1-*PV*, 10-*PV* and 20-*PV* of water injected). A constant flow rate of 5 cc/min was used during each stage of coreflooding, based on recommendations for stabilized flow. During CT-scanning, the core was scanned at the same locations (0.5-cm inter-slice distance). An image subtraction technique involving voxel-by-voxel subtraction of the CT-data for the core under vacuum from the image data for the various stages of displacement was used to view and quantify the fluid movement. The image subtraction and most of the post-processing work was done using the *VoxelCalc* software on a SUN Ultra-60 workstation.

Two different methods were used for calculating porosity (f) and porosity distributions using CT. The first of these methods, the standards method, involves scanning standards of known bulk densities and plotting bulk density versus CT numbers. The slope and the intercept of the straight-line fit are then used to compute the bulk density (r_{bulk}) of the unknown samples. Once the bulk density is known, porosity at each volume element (voxel) can be calculated using Equation 4.

$$f = \frac{r_{matrix} - r_{bulk}}{r_{matrix} - r_{fluid}} \quad \text{...} \; 4$$

The other method involves taking the scan of the core under vacuum and when it is fully saturated with brine, preferably containing a tracer such as sodium iodide. The equation used for calculating f is given below.

$$f = \frac{CT_{wet} - CT_{dry}}{CT_{water} - CT_{air}} \quad \text{...} \; 5$$

where, CT_{dry} and CT_{wet} are the mean CT numbers of the slice when the core is dry, and when it is saturated with brine containing a tracer, respectively. CT_{water} and CT_{air} are the mean CT numbers for the brine (containing tracer) and air, respectively. Details of both techniques can be found in the literature (Vinegar, 1986 and 1987; Withjack, 1988).

NMR measurements were made on 1.5" x 1.5" fluid saturated plugs in a Maran 2-MHz NMR instrument. Samples were wrapped in Teflon to minimize fluid loss during testing. The NMR signal was acquired using a CPMG (Carr-Purcell-Meiboom-Gill) pulse sequence acquiring 16,000 echoes with an inter-echo spacing of 0.10 ms. and a polarization time (delay time) of 7 s. Typically 150 scans were taken with a resulting signal-to-noise ratio greater than 50. The echo trains were processed using a BDR (Butler, Dawson and Reed) algorithm on the phase-rotated signal. Regularization in the inversion equations was based on the signal-to-noise ratio for each individual sample.

Heterogeneity measurements at whole-core and plug scales were computed using the Lorenz Coefficient (L_c) and the Dykstra-Parson's Coefficient (V_{DP}). The point permeability data used for calculation of the Lorenz Coefficients for the plug samples were obtained using the NER Autolab Permeability System. A total of 8 measurements on the surface of the plugs (45°-apart from one another) were taken at each location corresponding to a particular 0.5-cm thick CT-slice. The NMR-based Lorenz coefficients were calculated by ordering the surface-to-volume (S/V) ratio determined from the T_2 distributions with the porosity distributions determined from CT scans. The method is based on a simplification that the largest porosity intervals in the plug are most closely tied to the largest pore sizes.

Results and Discussion

Figures 2 and 3 are the CT-images of the slice porosities for the two carbonate plugs (#248 and #246) from Well A. The CT number data were used to generate bulk density data, which, in turn, were converted to porosities using the grain density data available from routine core analysis. In these figures, in order to enhance the contrast between the various parts of the slices, the smallest possible porosity range is used (0.15 to 0.30). The color legend is given in each figure at the top right-hand side. In these two figures brighter colors such as red and yellow represent a high porosity and darker colors such as black and blue represent a low porosity. The overall porosity distribution (for all the CT slices) is given at the bottom of the figure. The porosity variation along a diagonal line (usually from lower left to upper right-hand corner of the slice) on any interesting slice of each plug is given at the upper left-hand corner. The predominance of brighter colors in Figure 2 indicates that plug #248 is more porous than plug #246. The large variation of colors in Figure 2 also indicates that plug #248 may be more heterogeneous than plug #246. Conventional core analysis data on plug nos. 248 and 246 gave porosities of 0.291 and 0.228, respectively, with permeabilities of 961 md, and 648 md (at 2000 psig, room temperature), respectively.

Pore volume histograms for the two plugs together are shown in Figure 4. These are based on the voxel-by-voxel porosity data for all the slices of an individual sample plotted using 0.05% bin intervals. As shown in Figure 4, there is a slight difference between the porosity distribution and the PV-PHI distributions. Although CT-derived porosity data can be calculated for each voxel, their arithmetic average does not represent the true porosity. Therefore the term PV-PHI (or pore volume-weighted porosity) is

used, which gives a better estimate of porosities from the CT-derived data. The porosity and the PV-PHI histograms cross over at the porosity bin size of 0.25. The increase in the pore volume distribution is due to the fact that more of the pore volume of the sample is distributed in the portions of the sample with higher porosity. Discussions on PV-PHI can be found in the literature (Funk et al. 1999).

Figure 5 shows the PV-PHI histograms for the individual plugs (#248 and #246). The corresponding NMR T_2 distributions are shown in Figure 6. The T_2 distributions are typical of those seen in carbonates. In the absence of other data, the NMR distributions give a qualitative view of the plug sample heterogeneity but not a quantitative one. The samples are similar in that both show a large pore system (T_2 distribution peak at 1 s) connected with a smaller pore system (T_2 distribution peaks in the range of 90–300 ms). The distinction between the two pore systems is more pronounced in plug #248 than in #246. A third peak, seen at around 10 ms in the T_2 distributions for plug #248 is most likely related to a small micropore system, the existence of which is confirmed by the SEM images.

Figure 7 shows three fresh-break SEM snapshots (A, B and C) and a back-scattered image (D) taken from one end of Plug #248. The snapshot A shows the same breakdown in pore body sizes seen in Figure 6 - a large subsystem with a diameter of 70-100 m, a small subsystem with 10 m or smaller diameter and a very fine micro-crystalline subsystem. The snapshot B shows the limestone and dolomite crystals and the snapshot C shows the very fine calcite crystals contributing to the smallest pore sizes. The snapshot D shows the back-scattered image for the area shown in the snapshot C and it gives the maximum projection of 1.6, with an aspect ratio of 1.4.

A sequence of static data, similar to the ones for Well A, is shown for the three-plug set from Well B. Figure 8 shows the porosities of individual slices arranged in the composite core flood sequence (slices 1 through 7 representing Plug #26, 9 through 15 representing Plug #157, and 17 through 24 representing Plug #100, with slices 8 and 16 being the transition slices). The porosity values obtained from conventional core analysis (at 2500 psi and room temperature) for the three plugs in the above sequence are 0.281, 0.234 and 0.243, respectively, with corresponding permeability values of 476, 338 and 471 md. The CT-derived porosity values match nicely with the conventional data and maintain the order of porosities.

Figure 9 is the PV-PHI distribution for the individual samples based on CT data for the three plugs (eliminating the transition slices). Figure 10 shows the corresponding NMR T_2 distributions for the three plugs.

Dynamic two-phase data for the three-plug composite core from Well B are shown in Figures 11 and 12. Figure 11 represents the dynamic initial drainage data for 0.2-*PV* (pore volume) of injected oil and Figure 12 represents the dynamic drainage data at the end of a total of 20-*PV* of injected oil. In these two images, in order to enhance the

distribution of fluids inside the core, the matrix data were subtracted from the overall matrix and fluid data on a voxel-by-voxel basis. Additionally the matrix-subtracted oilflood CT data were subtracted from the CT data corresponding to 100% brine (sodium iodide doped) saturation. Details of the image subtraction technique used can be found in the literature (Siddiqui et al., 1999).

In Figure 11 the effect of heterogeneity on fluid flow is highlighted by the non-uniform oil saturation front (before oil breakthrough) after injection of 0.2-*PV* of oil (shown as red). The vertical cross-section of the core shows slight override of the oil between slices 11 and 13. More interestingly, both of these images show the presence of an unswept region (i.e. retention of water, shown as a blue diagonal line) between slices 1 and 8. The porosity distribution slices for the first plug (#26), as seen in Figure 8, did not show any unusually high- or low-porosity streaks. This heterogeneity in flow behavior, only seen during dynamic conditions, could not be predicted from the CT-derived porosity distribution alone. However, the NMR T_2 distributions may hold an important clue in this matter.

Figure 12 shows the same core at irreducible water saturation (after 20-*PV* of oil injection) with different plugs taking different amounts of oil. It also shows the existence of the unswept region, even after the injection of 20-*PV* of oil.

The conventional data for Well A showed that the L_c depends not only on the orientation of the tested samples but also on the size. As shown in Figure 13, the L_c varied from 0.74 for conventional horizontal plugs to 0.40 for whole core plugs, where the maximum horizontal permeability was used. The Dykstra-Parson's coefficient for the horizontal plugs from Well A was calculated to be 0.91 (highly-heterogeneous). The L_c for all the horizontal plugs from Well B was 0.75, very close to that for the horizontal plugs from Well A.

On the plug scale, the various techniques for determining the L_c provided very similar results. As expected, plug #248 from Well A was found to be more heterogeneous than plug #246. As shown in Figure 14, the L_c for plug #248 determined using the CT porosity distributions and the NMR T_2 distributions was 0.49, in close agreement with that determined from the use of CT-derived porosity and profile permeability data, where the L_c was 0.50 . Results were in similar close agreement for plug #246 from Well A. The *FZI*-based L_c for the two plugs was the lowest (0.21), among all the L_c values. It was calculated using CT-derived porosity data for the two plugs and the corresponding permeability transform in the form $k = a\, f^n$ (applicable to the two plugs for $3<FZI<6$).

Figure 15 shows that regardless of whether the porosity is determined by the CT standards method (Equation 4) or by the CT saturation method (Equation 5), the average porosity values are very close. The differences seen in plug #100 may be due to insufficient saturation with water for this highly heterogeneous plug. The C_v values from the CT number data for the saturation method are generally higher than those for the

standards method. In general, the more heterogeneous plug (#100) also has the highest C_v values for both methods.

What happens to C_v under dynamic conditions is generally a more complicated issue. It appears that C_v for this case is a function of the local heterogeneities as well as the type of fluids present in the core. Figure 16 shows the CT-derived saturation profiles inside the 3-plug composite core during various stages of coreflooding. The assumption used for generating this plot is that uniform saturation existed throughout the core at the end of water circulation following saturation (called 100% water shown in blue at the top) and at the end of 20-*PV* of oil (at irreducible water saturation of about 32%, shown in green at the bottom). It also shows the two other saturation conditions representing 0.2-*PV* of oil injected (shown in red and corresponding to Figure 11) and 20-*PV* of water injected (shown in brown, at residual oil saturation). The C_v values for the CT data used to generate Figure 16 are shown in Figure 17. In general, the lowest values of C_v are obtained for the highest water saturation inside the core and the highest values of C_v are obtained for the lowest water saturation.

Conclusions

1. The combination of CT and NMR data can reveal valuable information about porosity and pore-size distributions that play an important role in fluid flow characterization and reservoir performance prediction. The two methods are complementary and provide a synergistic improvement in reservoir characterization.

2. The combination of CT porosity distribution and NMR interpreted pore size distribution provides a convenient and accurate way to characterize the heterogeneity of individual core samples. This data can be critical for the comparison of two-phase flow and other displacement processes in porous media.

3. Simple porosity-mapped heterogeneity indicators are unable to capture the variability in saturation distributions for typical carbonate samples.

4. The coefficient of variation may hold important clues about the saturation conditions inside porous media in a multi-phase flow situation.

Acknowledgments

The authors wish to acknowledge the Saudi Arabian Ministry of Petroleum and Mineral Resources and the Saudi Arabian Oil Company (Saudi Aramco) for granting permission to present and publish this paper. The authors also wish to acknowledge their colleagues at the Petrophysics Unit and Sudhir Mehta at the Advanced Instruments Unit of Saudi Aramco Lab R&D Center.

Nomenclature

a	Coefficient used in the power-law fit of the f-k data	SR	Surface Relaxivity
C_v	Coefficient of Variation	S/V	Surface-to-Volume Ratio
E	Expected Value of a Random Variable x	T_1	Longitudinal Relaxation Time
FZI	Flow Zone Indicator	T_2	Transverse Relaxation Time
h	Reservoir or layer thickness	Var	Variance of a Random Variable x
k	Permeability	V_{DP}	Dykstra-Parsons Coefficient
L_c	Lorenz Coefficient	f	Porosity
n	Exponent used in the power-law fit of the f-k data	r	Density
PV	Pore Volume		

References

Bloembergen, N., Purcell, E. M., and Pound, R. V.: "Relaxation Effects in Nuclear Magnetic Absorption", Physics Review, 73, 1948, 679.

Craig Jr., F. F.: The Reservoir Engineering Aspects of Waterflooding, SPE of A.I.M.E., Dallas, 1971, pp. 64-66.

Funk J. J., Balobaid, Y. S., Al-Sardi, A. M. and Okasha, T. M.: Enhancement of Reservoir Characteristics Modeling, Saudi Aramco Engineering Report No. 5684, Saudi Aramco, Dhahran, November, 1999.

Kantzas, A: "Investigation of Physical Properties of Porous Rocks and Fluid Flow Phenomena in Porous Media Using Computer Assisted Tomography," *In Situ*, Vol. 14, No. 1, 1990, p. 77.

Jensen, J. L., Lake, L. L., Corbett, P. W. M. and Goggin, D. J.: Statistics for Petroleum Engineers and Geoscientists, Prentice Hall, Upper Saddle River, New Jersey, 1997, pp. 144-166.

Siddiqui, S.: Three Phase Dynamic Displacements in Porous Media, Ph.D. Dissertation, The Pennsylvania State University, University Park, PA, 1994.

Siddiqui, S., Khamees, A.A. and Velasco, V.B.: Three-Dimensional Relative Permeability and Dispersion Measurement using Computerized Tomography, Saudi Aramco Engineering Report No. 5687, Saudi Aramco, Dhahran, December, 1999.

Vinegar, H. J.: "X-Ray CT and NMR Imaging of Rocks," *Journal of Petroleum Technology*, March, 1986, p. 257.

Vinegar, H. J. and Wellington, S. L.: "Tomographic Imaging of Three-Phase Flow Experiments," *Rev. Sci. Instrum.*, January, 1987, p. 96.

Wellington, S. L. and Vinegar, H. J.: "X-Ray Computerized Tomography," *Journal of Petroleum Technology*, August, 1987, p. 885.

Withjack, E. M.: "Computed Tomography for Rock-Property Determination and Fluid-Flow Visualization," SPE paper 16951 presented at the 62nd Annual Technical Conference and Exhibition of the SPE in Dallas, Texas, September 27-30, 1987.

Withjack, E. M.: "Computed Tomography for Rock-Property Determination and Fluid-Flow Visualization," *SPE Formation Evaluation*, December, 1988, p. 696.

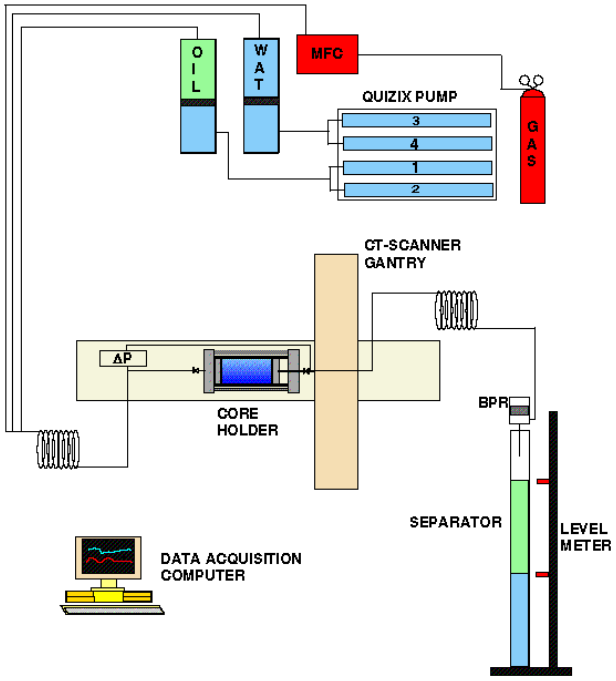

Figure 1: Schematic of the coreflooding system and the CT-scanner.

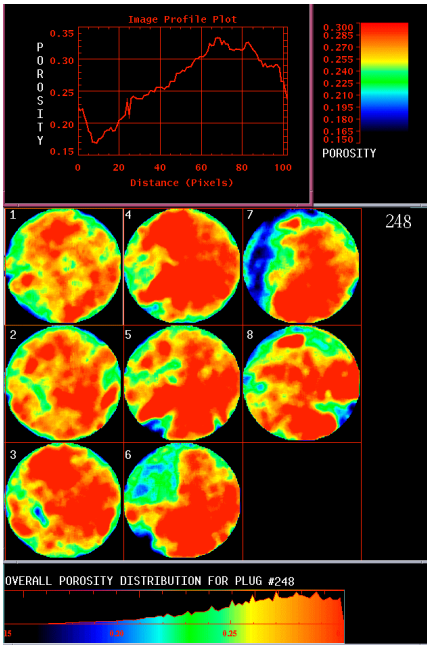

Figure 2: CT-images of the slice porosities for plug #248 from Well A.

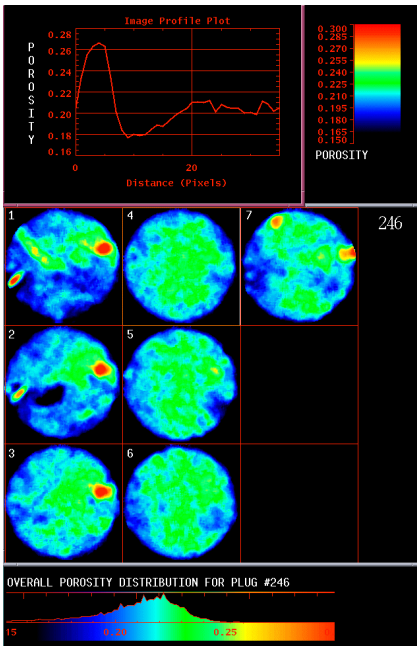

Figure 3: CT images of the slice porosities for plug #246 from Well A.

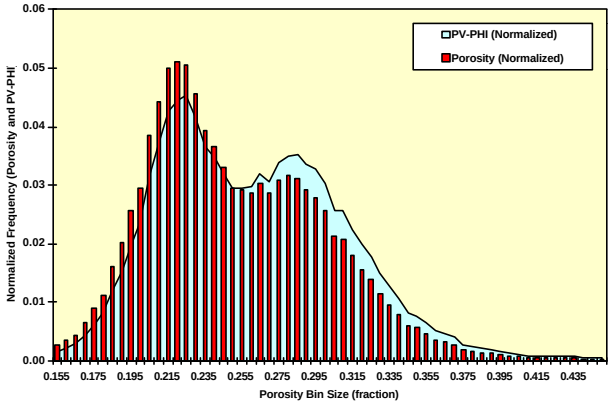

Figure 4: Porosity and PV-PHI histograms for both plugs (#248 and #246) from Well A.

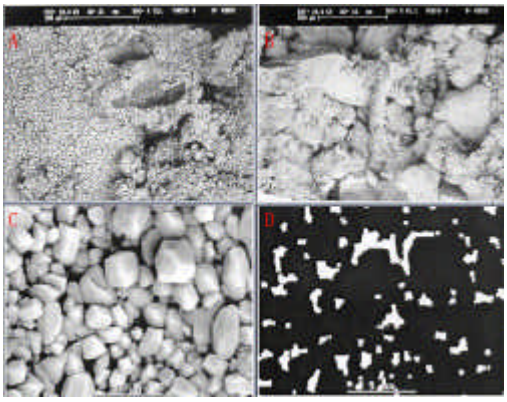

Figure 7: SEM images of the freshly-broken surfaces of plug #248 at different magnifications.

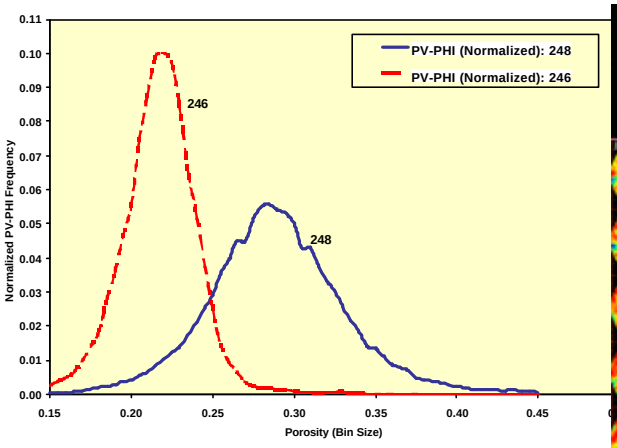

Figure 5: PV-PHI histograms for each of the individual plugs (#248 and #246) from Well A.

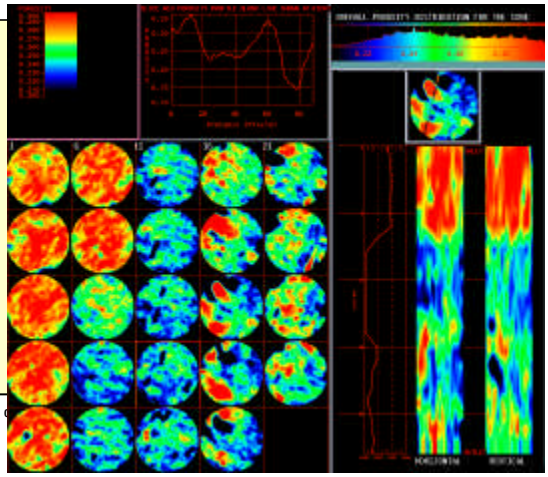

Figure 8: CT images of the slice porosities for the three plugs (#26, #157 and #100) from Well B.

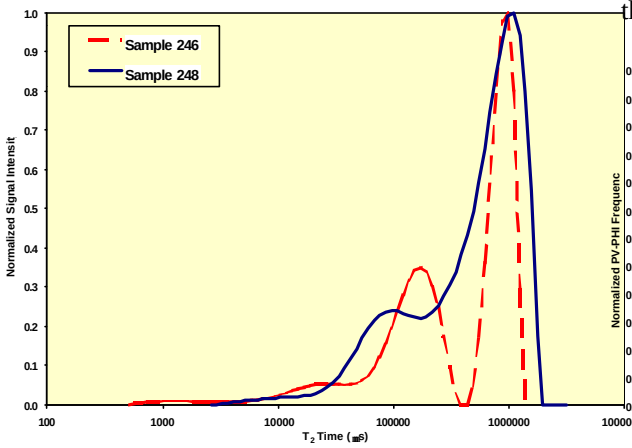

Figure 6: NMR T_2 distributions for each of the individual plugs (#248 and #246) from Well A.

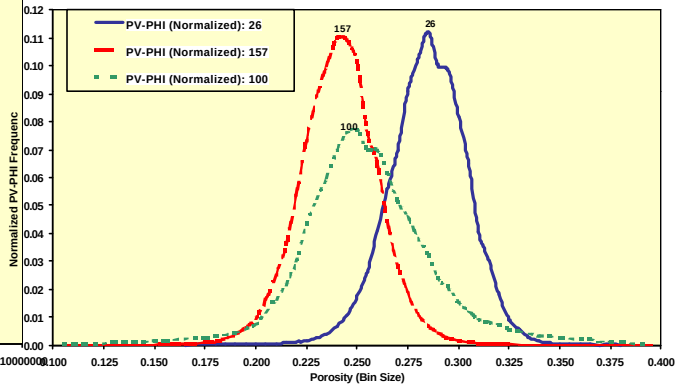

Figure 9: PV-PHI histograms for each of the individual plugs (#26, 157 and 100) from Well B.

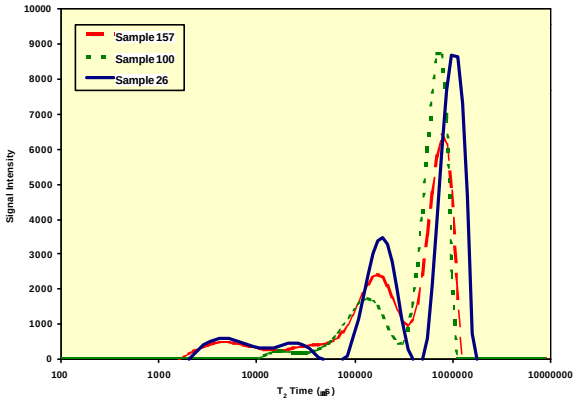

Figure 10: NMR T_2 distributions for each of the individual plugs (#26, 157 and 100) from Well B.

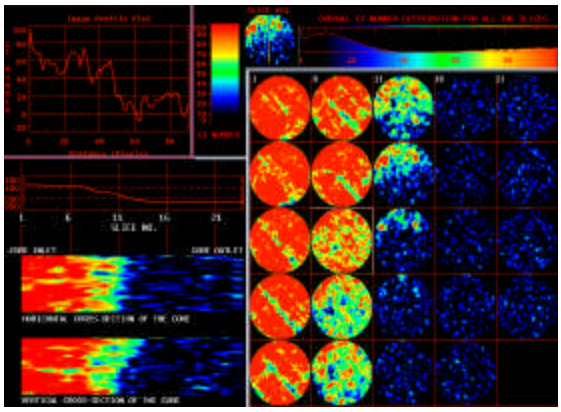

Figure 11: Matrix-subtracted CT images of the 3-plug composite core from Well B after 0.2 *PV* of oil is injected into the 100% water-saturated core.

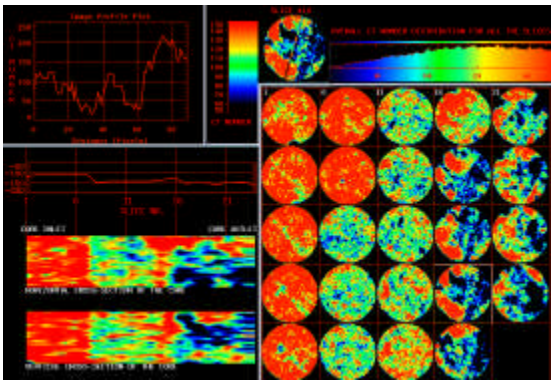

Figure 12: Matrix-subtracted CT images of the 3-plug composite core from Well B after a total of 20 *PV* of oil is injected into the 100% water-saturated core.

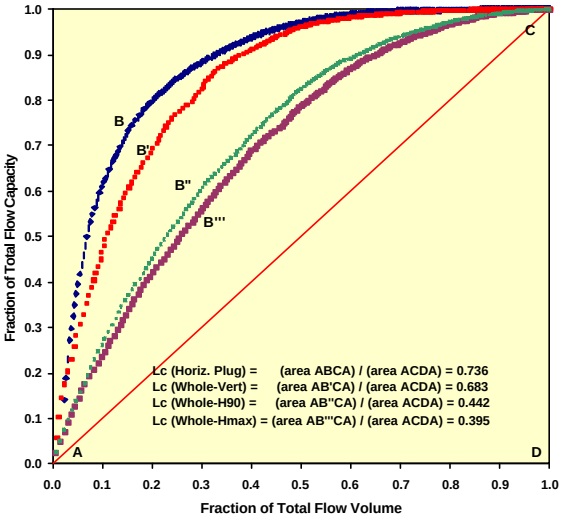

Figure 13: Stile's plot for Well A showing variations of L_c using various sources of conventional core analysis data.

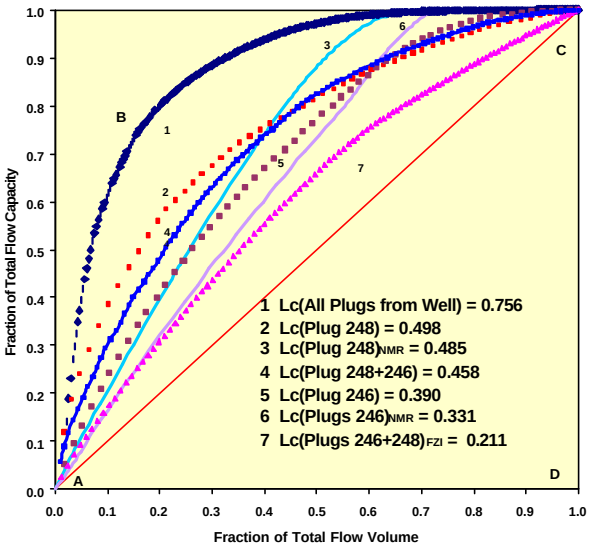

Figure 14: Stile's plot for Well A showing the variations of L_c values derived from individual plugs and their combinations using various CT and NMR-based techniques.

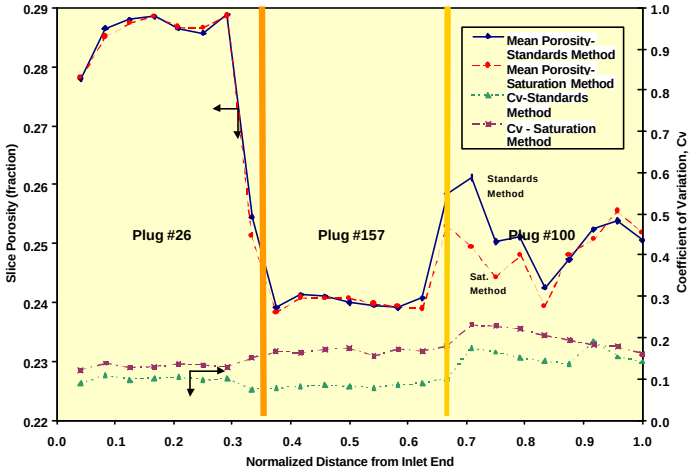

Figure 15: CT-derived average slice porosity values and C_v for the 3-plug composite core from Well B using the standard and the saturation methods.

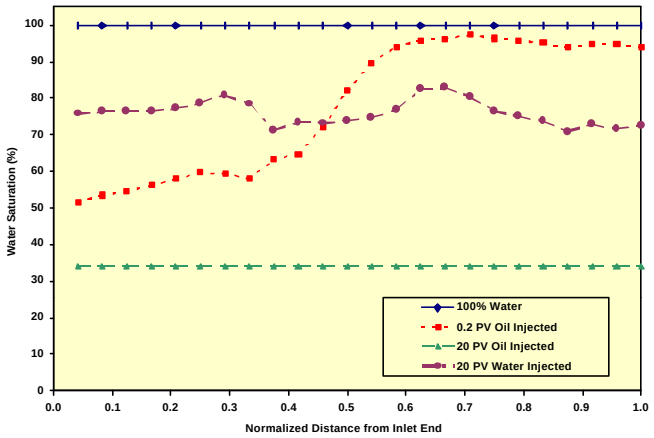

Figure 16: CT-derived saturation profiles for the 3-plug composite core from Well B during various stages of coreflooding.

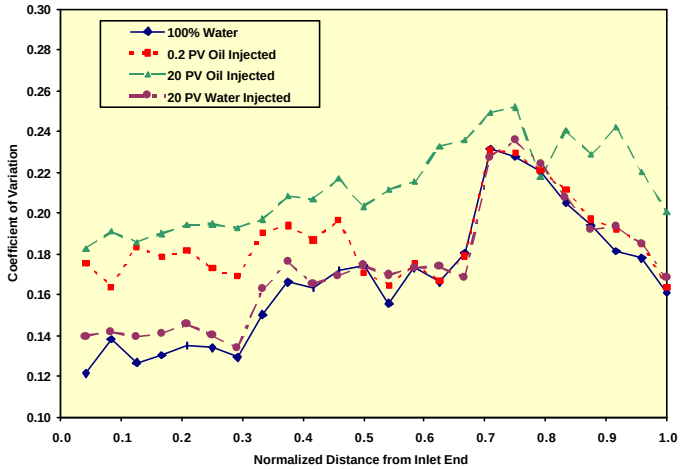

Figure 17: CT-derived C_v values used for saturation calculation for the same conditions as shown in Figure 16.